INTERNATIONAL JOURNAL OF CLIMATOLOGY, VOL. 17, 1301–1315 (1997)

MULTISCALE DETECTION OF ABRUPT CLIMATE CHANGES: APPLICATION TO RIVER NILE FLOOD LEVELS

KLAUS FRAEDRICH[1]*, JIANMIN JIANG[1]*, FRIEDRICH-WILHELM GERSTENGARBE[2] AND PETER C. WERNER[2]

[1]*Meteorologisches Institut, Universität Hamburg, Bundesstrasse 55, D-20146 Hamburg, Germany,* [2]*Potsdam-Institut für Klimafolgenforschung, Telegrafenberg, D-14473 Potsdam, Germany*

Received 28 November 1996
Revised 14 April 1997
Accepted 14 April 1997

ABSTRACT

The historical flood-level time series of the River Nile (AD 622–1470) is chosen to identify abrupt climate changes by applying global and local analysis techniques: the Mann–Kendall test and a non-hierarchical cluster analysis method to improve the Mann–Kendall test; a multiscale moving *t*-test with correction to the degree of freedom and an antisymmetric wavelet transform. The global estimates show three distinct epochs, AD 622–1078, 1079–1325 and 1326–1470, coinciding with larger scale climate changes: a relatively cool age, the Little Climatic Optimum of the Middle Ages, and an interim period before the Little Ice Age. The local estimates reveal the following results. The reference time of abrupt changes can be clearly identified, the associated time-scale coincides with the persistent anomaly period, and the maximum absolute *t*-value is statistically significant. There are about eight almost synchronous abrupt changes in the minimum and maximum River Nile flood levels, many of them are associated with 35–45 year persistence time-scales. An association of these short time-scales with those of interdecadal variability reported for the mid- and high-latitude sea-surface temperature of the North Atlantic is suggested, although information on phase coherence is not available. ©1997 by the Royal Meteorological Society. *Int. J Climatol.*, 17: 1301–1315 (1997)

(No. of Figures: 9 No. of Tables: 1 No. of References: 40)

KEY WORDS: River Nile; climate change detection; flood level record.

1. INTRODUCTION

Due to its obvious impact on nature and society, climate variability and change, especially abrupt climate changes, have been increasingly discussed in recent years (see, e.g. Berger and Labeyrie 1987). The time series of the minimum and maximum River Nile flood levels is a prime example for the study of climate change. The data set available covers a long time history (Said, 1993) and the geographical location, with its links to other climatic zones of the world, may represent a key region to demonstrate the possible global nature of climate variability. The Nile receives the water from the two main sources of the Blue and the White Nile in Ethiopia and equatorial Africa. The Nile flood maxima from the Blue Nile are related to the monsoonal rains in Ethiopia, associated with a northward shift of the intertropical convergence zone (ITCZ); the Nile flood minima originate in tropical East Africa.

The fluctuations of the Nile flood levels have been studied extensively since the reconstruction of the data set by Toussoun (1925) and Popper (1951). The analyses include long-term variability and non-linear scaling (Hurst *et al*, 1965), periodicities and trends (Brooks, 1927; Hassan, 1981; Hameed, 1984; Currie, 1987; Hassan and Stucki, 1987; Fraedrich and Bantzer 1991) and persistence (Popper, 1951; Riehl and Meitin, 1979; Evans, 1990). There are associations with climate variations in other regions of the world, with Europe, for example, and the El Niño–Southern Oscillation (Whetton *et al.*, 1990; Quinn, 1992), which is not surprising given the Nile's origin.

*Correspondence to: K. Fraedrich, Meteorologisches Institut, Universität Hamburg, Bundestrasse 55, D-20146 Hamburg, Germany
†Permanent affiliation: Beijing Meteorological College, 46 Baishiqiaolu, Beijing, 100081, P.R. China.
Contract grant sponsor: Klimavariabilität und Signal-Analyse.
Contract grant sponsor: Chinese national key Projects of Fundamental Research Programme on Dynamics and prediction Theories.

CCC 0899-8418/97/121301-15$17.50

The non-linear features of any abrupt change are also a relevant topic in other applied sciences (Yamamoto *et al.*, 1986). Karl and Riebsame (1984) identify the significant climate fluctuations in USA by using the Student *t*-test. Yamamoto *et al.* (1986) propose the concept of 'climate jump' and deduce a criterion based on the *t*-test. Goossens and Berger (1987) introduce the Mann–Kendall rank test for detection of abrupt climatic change. Jiang and Liu (1993) and Jiang and You (1997) compare the above-mentioned three methods by applying them to the atmospheric dryness index over mainland China, and conclude that the *t*-test at the confidence level $\alpha = 0{\cdot}01$ coincides approximately with Yamamoto *et al.* (1986) climatic jump criterion and with the Mann–Kendall test (Goossens and Berger, 1987) at the confidence level $\alpha = 0{\cdot}05$.

In this note various methods of estimating climate change are introduced and applied to the River Nile flood-level record. Section 2 provides some statistical background information on the data set before, in section 3, global and more dynamically oriented local estimates of climate change are utilized. Conclusions follow in section 4.

2. NILE RIVER FLOOD LEVELS: A STATISTICAL CLIMATOLOGY

The flood level data at Roda Island are analysed for the period from AD 622 to 1470 (see Figure 1 of Fraedrich and Bantzer, 1991). The missing data in individual years are linearly interpolated. The statistical setting of the River Nile flood-level record is represented by distributions and extremes. Comparison of the absolute frequency distributions of the minimum and maximum flood levels (Figure 1(a and b)) reveals that there is a difference of the underlying climatology. That is, the Ethiopian monsoonal precipitation feeding the Blue Nile and the East African rains generating the White Nile. This is substantiated by the natural extreme value region (NER), defined as the upper and lower area of the distribution (see Gerstengarbe and Werner, 1989), where values differ significantly from the remainder of the distribution. The upper NERs of both the minimum and maximum levels, especially exhibit a significant difference in structure; the associated evolution is shown by the time series of the smallest and largest values (for 50-year intervals; Figure 2(a and b)). There is an increase in the largest values (especially towards the end of the time series) and a parallel decrease in the smallest values for the maximum flood levels in this period, which may be related to the effect of sedimentation.

The following section will focus on abrupt changes in both minimum and maximum flood-level time series. The influence of siltation is not excluded, because the same order of magnitude of the total increase occurs in both the maximum and the minimum flood levels (Popper, 1951).

3. NILE RIVER FLOOD LEVELS: ABRUPT CHANGES

Climate change detection techniques are applied to both the minimum and maximum River Nile flood-level time series. *Global* statistical estimates are based on the Mann–Kendall test (Sneyers, 1975; Goossens and Berger, 1987) and a non-hierarchical cluster analysis algorithm (Appendix A); note that this type of Mann–Kendall test is a progressive analysis which tests the beginning of a single trend within a sample based on the progressive and retrograde rank series. More dynamically oriented *local* estimates utilize the wavelet-transform (Hagelberg and Gamage, 1994; Mahrt, 1991; Mallat and Zhong, 1992; Collineau and Brunet, 1993; Brunet and Collineau, 1994; Gamage and Hagelberg, 1993; Hagelberg and Gamage, 1994; Appendix B) and the multiscale moving *t*-test; note that, in comparison with the wavelet transform, the multiscale moving *t*-test is not a tool of decomposition owing to the second moments being involved.

3.1. Global estimates

There are various criteria of the Mann–Kendall rank test for the detection of multiscale abrupt changes in a longer time series and those abrupt changes that are similar to an asymmetric Gaussian function. The typical criterion of the Mann–Kendall test seems suitable to detect only one abrupt change in a given time series and to detect changes of persistent anomalies that are of a Gaussian type. Applying the Mann–Kendall test to the Nile flood levels (Figure 3) yields one abrupt change around AD 1020 in the minimum flood levels; other changes are not significant but may be identified as intersections outside the 5 per cent significance levels and some uncertain

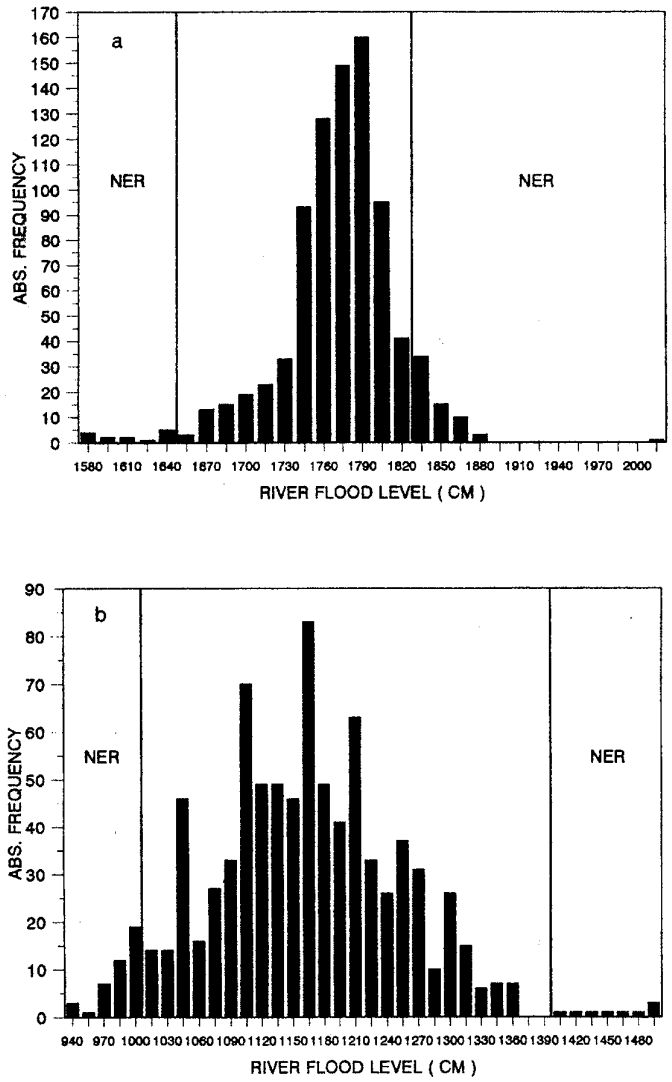

Figure 1. Frequency distributions of the (a) maximum and (b) minimum River Nile flood levels for the period AD 622–1470

extreme on the solid lines (associated with the maximum and minimum floods). However, a non-hierarchical cluster analysis, applied next, may improve the estimates.

The application of the non-hierarchical cluster analysis algorithm (Appendix A) requires the definition of the number of elements to be analysed, which, in the case of the Nile data, is the number of years of the time series (AD 622 to 1470). Each element is described by a set of three ($N=3$) parameters, p: the minimum and the maximum flood levels and their difference, which are individually normalized by the z-transformation. Applying the cluster analysis leads to nine clusters, each containing a number of years of similar structure of the parameter set used. Then, after sorting the clusters by the magnitude of the group centroids (A2), each cluster (that is, each element within the cluster) can be marked by a characteristic number, say -4 to $+4$. The resulting time series is shown in Figure 4(a) using a 21-year running mean (full curve). A first interpretation of this curve leads to the following results. The period between AD 622 and 1470 is characterized by a number of abrupt changes. There are three clearly distinct epochs: 622–1078, 1079–1325 and 1326–1470, with different long-term means increasing with time. They are similar to those obtained by the Mann–Kendall test (Figure 3), although based on different

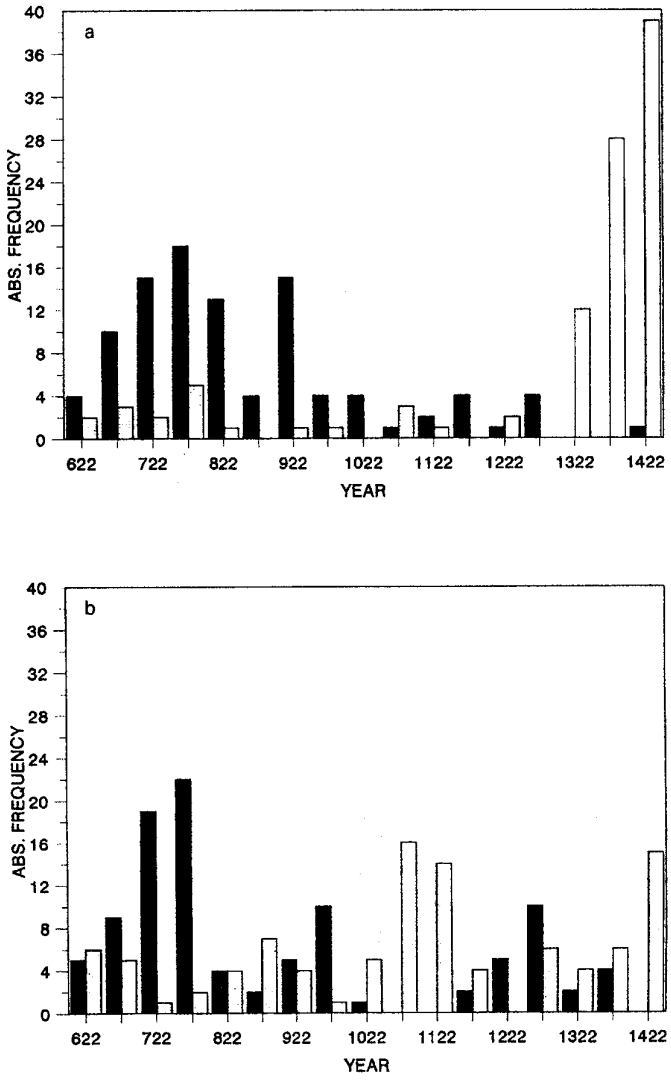

Figure 2. Smallest (black columns) and largest (stippled) values of the (a) maximum and (b) minimum River Nile flood levels (absolute values are taken from 50-year intervals)

criteria and variables (i.e. on both maximum and minimum flood levels). This leads to the question: Is there the beginning of a trend, if the parameters are regarded as a complex quantity? Subjecting the calculated cluster values to the Mann–Kendall test shows (Figure 5(a)) only one starting point for the development of a trend at AD 1032, which is statistically safe. Only two periods are clearly defined as climatic trends of the River Nile flood levels. In connection with the results presented in Figure 3, the changes of the maximum flood levels appear to be more important than those of the minimum. This is supported by an additional application of the Mann–Kendal test to the period AD 622–1300. Again, in this case the starting point of a development of a trend occurs at AD 1032 (Figure 5(b)), which is in a good agreement with the result of the Mann–Kendall test applied to the minimum flood level (Figure 3(b)).

The observed separation of the periods AD 622–1078 and 1079–1325 (and possibly 1326–1470) in the River Nile flood levels can also be detected in climatological time series in Europe. For example, the series of the dry

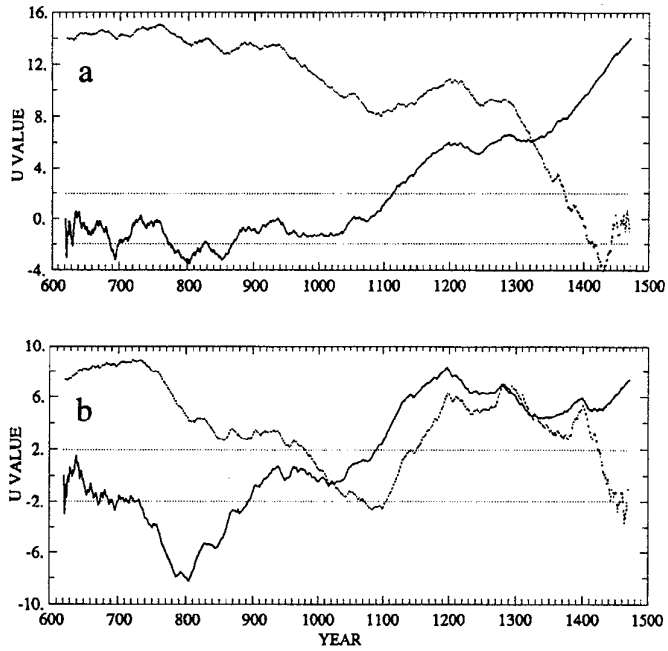

Figure 3. The Mann–Kendall test on the Nile maximum (a) and minimum (b) levels

mass of the sediments of the Holzmaar (Eifel, Germany) shows significantly different behaviour before AD 1079 (compared with after 1079, Figure 4(b); the epoch between 1079 and 1375 has distinctly higher values and a larger variance. Similar results are obtained by Stuiver and Quay (1980) from tree-ring analysis, and by Bernhardt and Mäder (1987) for the number of warm and dry summers. These climate epochs coincide with the so-called Little Climatic Optimum of the Middle Ages between AD 1100 and 1300. Its end, near AD 1300, which is identified in the same manner (Figures 4(a and b) and 5(a)), characterizes the beginning of an interim period between the Little Climatic Optimum and the Little Ice Age (AD 1500 to 1900). The flood-level epoch from AD 622 to 1078 may be representative of a relatively cool age in Europe (which is also reported for Japan). That is, the climate changes noted in the Nile flood levels are not confined to north-east Africa, but may be part of a large-scale pattern of the global climate system, in particular, when given the links between the Nile flood variability and the El Niño–Southern Oscillation phenomenon (Whetton *et al.*, 1990; Quinn, 1992). These parameter-free tests will now be supplemented by local methods: the wavelet transform and the multiscale moving *t*-test.

3.2. Local estimates

The first derivative Gaussian (FDG) wavelet transform of the Nile flood levels is shown for the minimum and maximum levels (Figure 6(a and b)). The vertical axis is represented by octave scaling of the years to make smaller scale variability more visible. A positive centre denotes an apparent increase of the flood levels, and vice versa. Changes on the largest scale, of about 300–400 years, are notable around AD 980 in the minimum flood levels, and around 1110 in the maximum flood levels. Changes on century scales occur around AD 700, 940 and 1195 as decreasing minimum flood levels, and around AD 820, 1055 and 1370 as increasing minimum flood levels. These results are almost consistent with Fraedrich and Bantzer's (1991) analysis obtained after low-pass filtering of the data. There is only one change on the century scale, detected near AD 1340 when the maximum flood levels increase almost synchronously with the minimum flood levels (around 1370). Meanwhile, weaker changes of decreasing maximum flood levels are discovered around AD 940 and 1195 on decadal scales. Furthermore, approximately synchronous changes in both minimum and maximum flood levels are noted on the

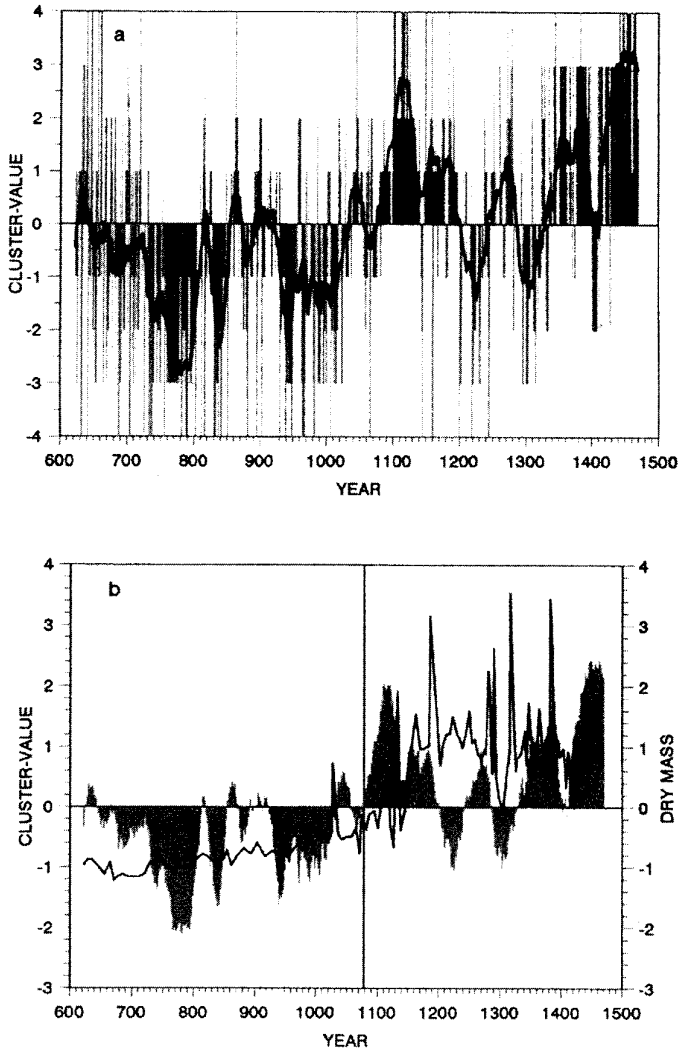

Figure 4. (a) Time series of cluster values (nine clusters ranging from -4 to $+4$) of the transformed river Nile flood levels (vertical lines) and the running mean (thick curve). (b) Normalized and averaged (11-year running mean) cluster values of the transformed River Nile flood-level parameters (shaded) and the dry mass in the Holzmaar sediment (full black line)

decadal time-scale around AD 760, 828 and 1290 with decreasing levels, and around 850, 952 and 1245 with increasing levels. In general, more changes occur in the minimum flood levels than in the maximum ones. The Haar wavelet transform displays patterns that are very similar to those of the FDG transform, but with less smooth contours (not shown).

The multiscale moving *t*-test is applied next. here the idea is to test the difference between two subsamples before and after the change point with equivalent subsample size (persistence time scale or duration) $n = n_1 = n_2$. For a sample whose population is normally distributed, the *t*-statistic is calculated as follows:

$$t(n, i) = (x_{i2} + x_{i1})\, n^{1/2}\, (s_{i2}{}^2 + s_{i1}{}^2)^{-1/2}$$

with

$$x_{i1} = {}_{j=i-n}\Sigma^{i-1} x_j/n,\ x_{i2} = {}_{j=i}\Sigma^{i\,n-1} x_j/n,\ s_{i1} = {}_{j=i-n}\Sigma^{i-1}(x_j - x_{i1})^2/(n-1),\ s_{i2} = {}_{j=i}\Sigma^{i+n-1}(x_j - x_{i2})^2/(n-1)$$

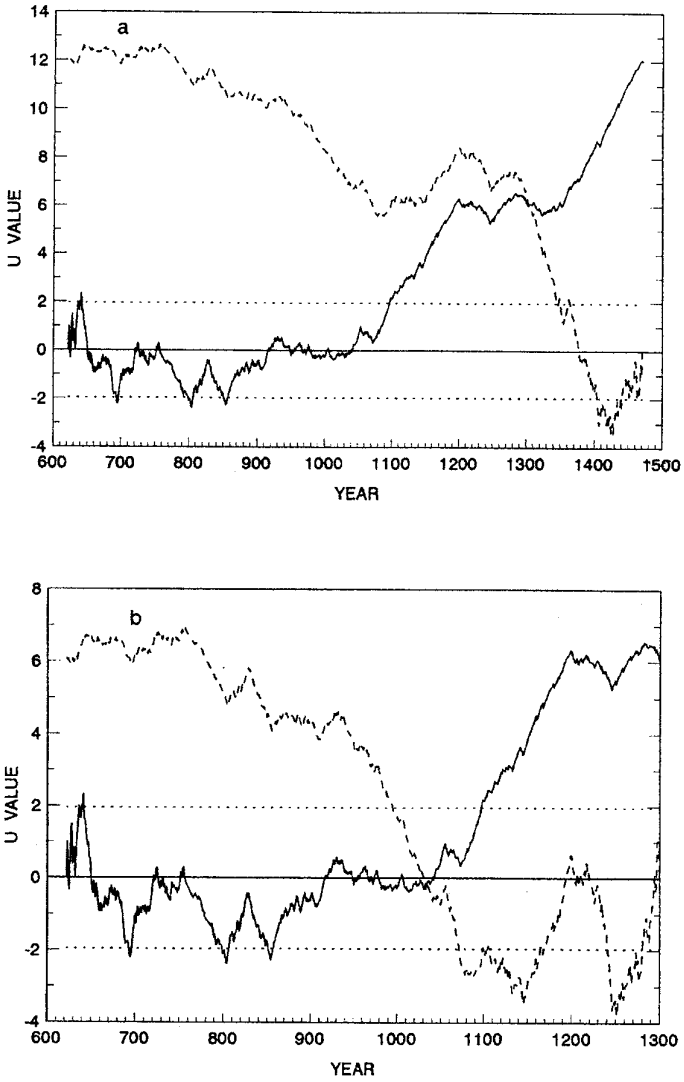

Figure 5. Mann–Kendal test on cluster values of the transformed Nile River flood-level parameters (a) for the period AD 622–1470 and (b) for the period AD 622–1300

Multiscaling is achieved by varying $n=2, 3, \ldots, <N/2$, and moving $i=n+1, n+2, \ldots, N\text{-}n$, Note that in comparison with the wavelet transform, the multiscale moving t-test is not a tool of decomposition due to the second moments, s_{i1} and s_{i2}, being involved.

The results of the multiscale moving t-test of the Nile flood levels are shown for the maximum and minimum levels after smoothing the contours by a low-pass filter (Figure 7(a and b)), for which we have applied a Gaussian function of zero mean and standard deviation 0·5 $[0{\cdot}7+(k-1)/2]$ at the weighting points $k=1+2\ (n/10)$ for $n \leq 80$, and $k=17$ for $n>80$. It shows successfully, patterns very similar to those of the wavelet transform, with apparent rides of the maximum absolute t-values stretching vertically along the reference years of abrupt changes. A t-test is performed including a correction to the degrees of freedom associated with the time series to exclude the effect of autocorrelation. The 'effective' degrees of freedom are estimated for unfiltered t-values corresponding to the centres of the maximum absolute t-values (Figure 7(a and b)). The following results are noted: abrupt flood-level changes occur synchronously in both the maximum and minimum flood levels. For

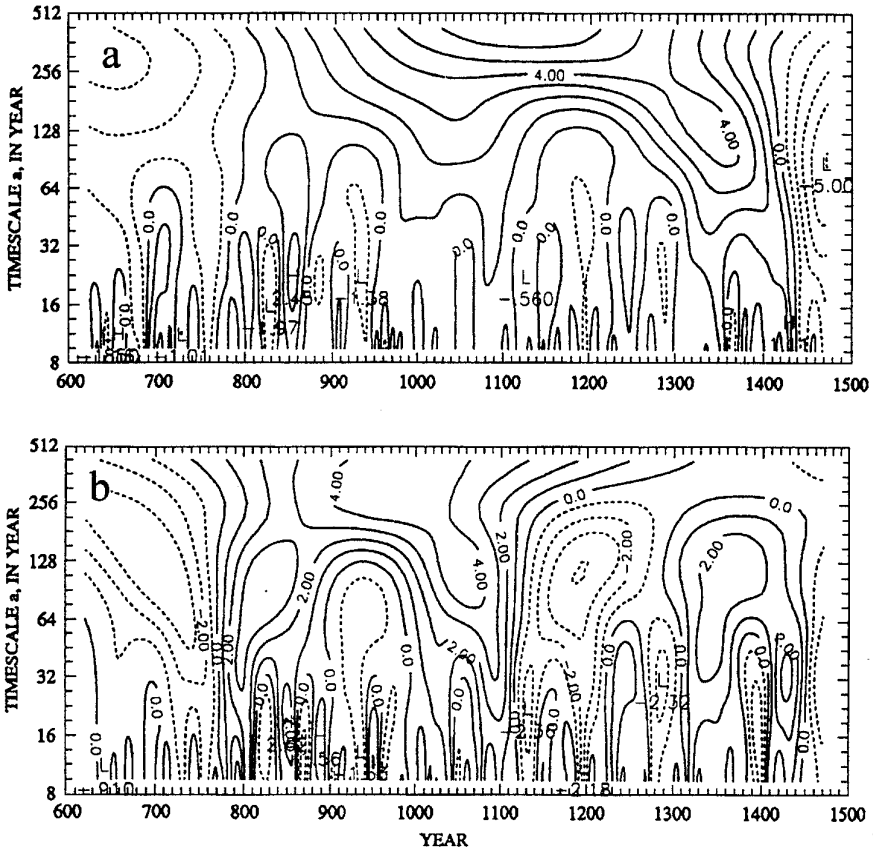

Figure 6. The first derivative Gaussian wavelet transform of the (a) maximum and (b) minimum Nile flood levels

instance, the significant changes around AD 759, 1075, 1096, 1195, 1246, 1284, 1322 and 1342 are associated with time-scales of climate changes lasting longer than 35 years. They are almost synchronous in both of the maximum and minimum flood levels and marked as 'S' in Figure 7(a and b). There are also asynchronous changes occurring preferably in the minimum levels. They are associated with various time-scales and marked as 'A' in Figure 7(a and b). All significant (on the level $\alpha<0{\cdot}01$) changes are listed in Table I.

Table I contains the reference year of the detected abrupt change (year of change), the subsample size (time-scale), the mean of the subsample before the year of change (Mean 1) and its standard deviation (SD 1), the mean of subsample after the year of change (Mean 2) and its standard deviation (SD 2), the unfiltered t-value, the 'effective' degrees of freedom (EDF), and the corresponding $t_{0{\cdot}01}$ value in the right column. The upper part lists the eight pairs of abrupt changes. They are almost synchronous in both the maximum and the minimum flood levels, with almost the same year of change but somewhat different time-scales of duration. The bottom part identifies the asynchronous changes. They occur only in the maximum flood levels (middle) or in the minimum flood levels (lower part). For example, the change year AD 759 in the maximum flood levels is associated with two subsamples; a comparatively high subsample mean level 17·59m (Mean 1) with standard deviation 0·38 m (SD 1) covering the period from AD 714 to 758 (a wet climatic spell of 45 years), and a comparatively low subsample mean 17·22 m (Mean 2) with standard deviation 0·40 m (SD 2) covering the consecutive period from AD 759–803 (a dry climatic episode of 45 years). The t-value $-4{\cdot}55$ means an abrupt drop of the flood levels around AD 759 at the confidence level exceeding well beyond $\alpha=0{\cdot}01$ ($t_{0{\cdot}01}=-3{\cdot}25$) with EDF = 9.

There are three time-scales of climate changes shown in Table I. Most of the synchronous changes occur on time-scales of 35–45 years duration followed by the duration of 117–128 years. The longest time-scale of 395

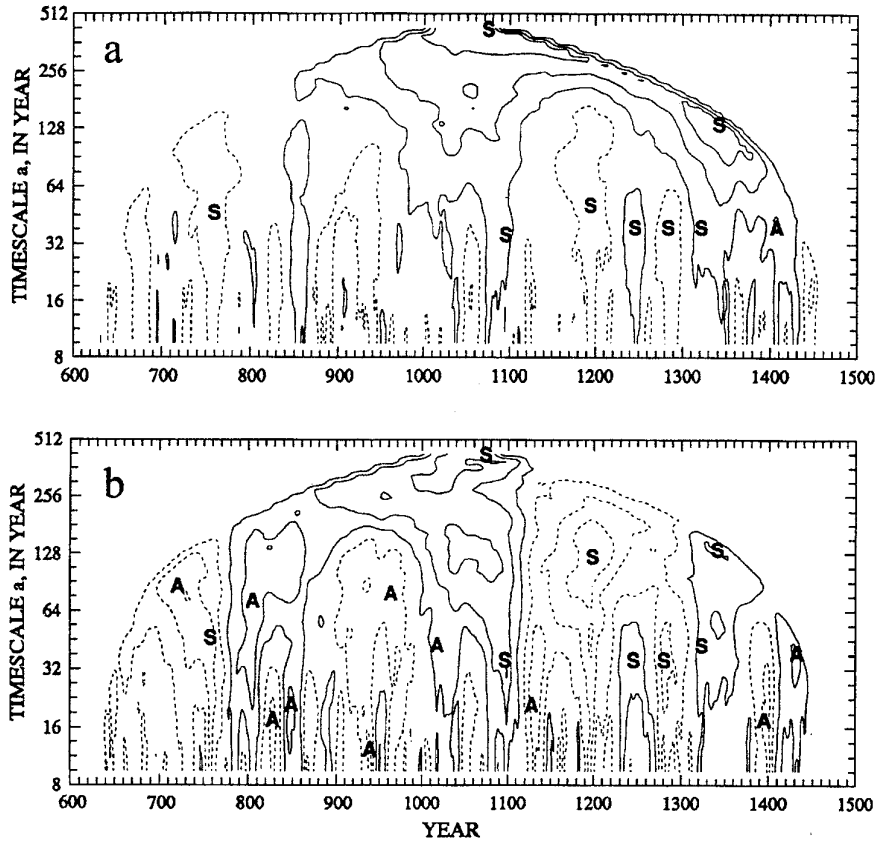

Figure 7. The low-pass multiscale moving t-test on the Nile maximum (a) and minimum (b) levels. The interval of contours is 3 with $-7, -4, -1$ in dashed lines, and 2, 5, 8 in solid lines. 'S' denotes the almost synchronous change in both the maximum and minimum flood levels. 'A' indicates the change merely in the corresponding series

years is also highly significant, which the FDG wavelet transform fails to detect. Six of eight synchronous changes are observed between AD 1060 and 1470, coinciding with the 'little or secondary climatic warm epoch' in Europe (Hassan, 1981). Only one asynchronously abrupt change is found in the maximum flood levels, whereas 10 asynchronously abrupt changes occur in the minimum flood levels. The reason is that the maximum flood levels have weaker fluctuations on shorter time-scales. In addition, all EDF are much smaller than the corresponding subsample size (duration or time-scale), which is due to the strong autocorrelation in the Nile floods, especially in the maximum levels.

The abrupt simultaneous changes around AD 1246 and 1281 (Table I) are roughly consistent with Popper's (1951, table 27) corresponding subperiod of decades; however, the changes around AD 1097 and 1324 are not noted in Popper's table. Other synchronous changes (noted in Table I) are similar to Popper's analysis but related to different time-scales. In general, it appears that the dates presented in Table I reveal higher time resolution and are objectively determined. The reference year 1284 of the synchronous changes and changes around AD 805 and 849 in the minimum levels coincide with the determination of the short-period fluctuations in the maximum flood levels noted by Riehl and Meitin (1979) with different durations. Furthermore, some change trends listed in Table I are consistent with Said's (1993) description, especially for the jump of the flood levels around AD 1096. The episode of AD 1061–1095 was characterized by severe drought, famine and significant population reduction in Egypt, whereas the spell of AD 1096–1130 was characterized as normal with good floods, contemporaneous with warmer temperature and frequent droughts in Europe (Said, 1993, pp. 164–166).

Table 1. Significant abrupt changes in the Nile river flood levels

Maximum and minimum	Year of change (AD)	Time-scale (years)	level before the year (m)		Level after the year (m)		t value	$t_{0.01}$ value	EDF
			Mean 1	SD 1	Mean 2	SD 2			
Maximum	759	45	17·59	0·38	17·22	0·40	− 4·55	− 3·25	9
Minimum	758	45	11·09	0·71	10·23	0·49	− 6·70	− 2·98	14
Maximum	1075	395	17·46	0·42	17·83	0·37	13·28	2·66	77
Minimum	1074	395	11·24	0·85	11·81	0·89	9·21	2·62	135
Maximum	1096	35	17·58	0·22	17·79	0·18	4·44	3·50	7
Minimum	1097	35	11·72	0·58	12·83	0·65	7·49	3·01	12
Maximum	1195	49	17·80	0·21	17·55	0·36	− 4·09	− 3·36	8
Minimum	1199	117	12·27	0·66	11·32	0·76	− 10·28	− 2·70	39
Maximum	1246	38	17·54	0·26	17·80	0·17	5·11	3·71	6
Minimum	1246	35	11·16	0·65	11·86	0·50	5·03	3·11	11
Maximum	1284	38	17·80	0·17	17·60	0·24	− 4·31	− 3·50	7
Minimum	1281	35	11·86	0·71	11·00	0·77	− 5·55	− 3·17	10
Maximum	1322	38	17·60	0·24	17·85	0·24	4·57	3·50	7
Minimum	1324	41	10·97	0·75	11·65	0·87	3·80	3·01	13
Maximum	1342	128	17·67	0·24	18·12	0·35	12·02	2·81	23
Minimum	1342	128	11·32	0·76	11·98	0·92	6·18	2·70	42
Maximum	1407	38	17·99	0·29	18·33	0·25	5·56	3·50	7
Minimum	721	83	11·48	0·92	10·57	0·64	− 7·43	− 2·79	25
Minimum	805	70	10·44	0·61	11·48	0·84	8·41	2·82	22
Minimum	828	17	11·64	0·55	10·74	0·30	− 5·96	− 4·60	4
Minimum	849	21	10·79	0·30	12·04	0·82	6·55	4·60	4
Minimum	939	12	11·59	0·48	10·57	0·41	− 5·63	− 4·60	4
Minimum	963	76	11·58	0·75	11·15	0·70	− 3·64	− 2·78	26
Minimum	1018	41	10·97	0·64	11·68	0·70	4·75	2·98	14
Minimum	1128	21	12·94	0·49	11·96	0·67	− 5·45	− 3·71	6
Minimum	1395	17	12·28	0·51	10·96	0·90	− 5·25	− 4·60	4
Minimum	1432	38	11·36	0·86	12·60	0·81	6·48	3·01	13

A pair of examples of abrupt increases is illustrated in Figure 8(a and b): one case occurring around AD 1246 in both the minimum and the maximum flood levels. The upper panels are the annual minimum (Figure 8(a)) and the maximum (Figure 8(b)) flood levels; the thin horizontal lines indicate the subsample means. The middle panels are the moving t-values unfiltered and subtracted from the whole series on subsample size $n = 35$ in the minimum, $n = 38$ in the maximum flood levels. The bottom panels show the Mann–Kendall test on the corresponding period of this pair of examples.

These synchronous abrupt changes in both of the minimum and the maximum flood levels suggest that the changes on longer time-scales are probably controlled by some type of variation on larger spatial and longer temporal scales in the climate system, for example, the world-wide anomalies of the SST (Folland *et al.*, 1986; Kushnir, 1994) and the West Atlantic (WA) pattern in the summer (Jiang and Qian, 1994), although fluctuations in individual years are less correlated between each other (Popper, 1951; Evans, 1990; Conway and Hulme, 1993).

4. CONCLUSIONS

Two historic time series of maximum and minimum flood levels of the Nile River are analysed for abrupt climate changes by applying various techniques: Mann–Kendall test, a non-hierarchic cluster analysis, and locally resolving methods, the wavelet transform and a multiscale moving t-test with correction to the degrees of

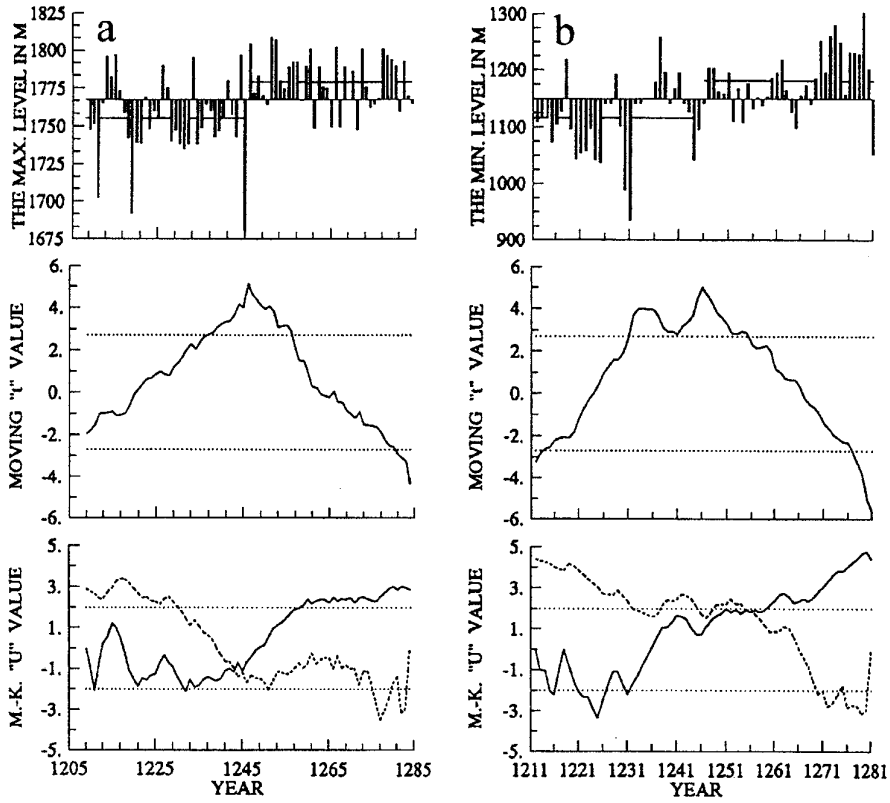

Figure 8. A pair of examples of abrupt changes in both the maximum (a) and minimum (b) flood levels of the Nile

freedom. A list of significant abrupt changes of the Nile floods is established. The main conclusions are as follows.

The typical criterion of the Mann–Kendall test appears to identify only one abrupt change in a given time series and to detect changes of persistent anomalies of Gaussian type. The cluster analysis provides further details and, furthermore, identifies the Nile maximum flood level as the leading parameter within the development of the characteristic trend in the period analysed. The multiscale moving *t*-test technique has the following advantages over the antisymmetric wavelet transform for identifying multiscale abrupt changes in longer time series. The reference time of the abrupt change detected is clearly centred on the actual time point. The time-scale revealed coincides with the persistent period of the time series more accurately. More importantly, the maximum absolute *t*-values provide the levels of statistical significance for the abrupt changes, which the wavelet transform does not. Therefore, this multiscale moving *t*-test may be applied to turbulence and other normally distributed signals.

The global estimates of climate change in flood levels reveal basically three climate epochs of longer time-scales, AD 622–1078, 1079–1325 and 1326–1470, coinciding with larger scale climate changes reported in Europe: a relatively cool age, the Little Climatic Optimum of the Middle Ages, and an interim period before the Little Ice Age. The local analysis reveals eight pairs of abrupt changes in the minimum and maximum flood levels, which occur almost synchronously and many of them are related to the 35–45 year time-scales of persistence. Note that some of the changes identified here coincide with results described by Popper (1951) and Said (1993); three reference years of abrupt change are consistent with Riehl and Meitin (1979), but the related time-scales do not coincide with their analyses. It is suggested that these short time-scales of persistence can be associated with similar magnitudes representative of the interdecadal variability reported for the mid- and high-latitude sea-surface temperatures of the North Atlantic (and the related atmospheric patterns, see Kushnir 1994), although information on phase-coherence is not available.

ACKNOWLEDGEMENTS

This work is partly supported by the Climate Program 'Klimavariabilität und Signal-Analyse' of Germany, and by the National Natural Science Foundation of China. The Holzmaar time series was kindly made available by Professor Dr J. F. W. Negendank (Potsdam, GeoForschungsZentrum). One of us (KF) has gained considerably from the stimulating discussions with Professor Rushdie Said. The comments of two referees are appreciated.

APPENDIX A

The extended non-hierarchical cluster analysis method

Cluster analysis procedures enable several coherent parameters to be evaluated on a distribution-free basis, and patterns to be identified. This is due to their transparency and the multifarious ways in which they can be applied. The following investigations are carried out using non-hierarchic cluster procedures (Steinhausen and Langer, 1977). The principle of this analysis can be described as follows:

(i) definition of each element, e_i by a number, N, parameters, P;
(ii) determination of an initial partition by sorting the elements on the basis of the parameters into a defined number of, k, clusters;
(iii) calculation of the group centroid, $\bar{e}_m$;
(iv) euclidian distance calculation of the target function $z(g)$ for each grouping step, g:

$$z(g) = \sum_{m=1}^{k} \sum_{i \in m} |e_i - \bar{e}_m|^2 \tag{A1}$$

(v) realization of grouping—a grouping step can be understood as the shifting of the elements, e_i into the cluster with the nearest centroid, e_k, with respect to the Euclidian distance;
(vi) minimizing the target function $z(g)$ $\forall g \Rightarrow min$.

The target function reaches a local minimum if two successive grouping steps are equal. In this case, the iteration procedure will be interrupted, because the optimum classification for the given number of clusters has been obtained. Now, each cluster contains a number of L elements, which, in general, is different from cluster to cluster. Although the cluster analysis has been completed, the number of clusters is not necessarily optimal. This requires an extension of the cluster analysis (Gerstengarbe and Werner, 1997): normally an absolute separation of the clusters is not possible under the condition of a well-defined number of clusters. In this case so-called 'overlaps' between the parameters of the clusters in the n-dimensional space exist. These 'overlaps' can serve as a starting point to answer questions as to the quality of the cluster separation and, in connection with this, as to the optimum number of clusters. The basic idea is as follows:

First, the number of 'overlaps', $U_{a,b}$, between two clusters a and b can be calculated as

$$U_{a,b} = \sum_{i1=1}^{La} \sum_{i2=1}^{Lb} \sum_{J=1}^{n} u_{i1,i2j}, \quad a = 1, \ldots, k-1; b = 2, \ldots, k \tag{A2}$$

and the condition $\bar{e}_1 > \bar{e}_2 > \cdots > \bar{e}_k$

with $u_{i1,i2,j} = 1$ for $P_{i2,j} > P_{i2,j}$, $u_{i1,i2,j} = 0$ for $P_{i2,j} \leq P_{i2,j}$; and an absolute separation for $U = 0$. Second, estimating the maximum possible number of 'overlaps' by $U_{\max} = n\ (L_a L_b - 1)$. Finally, using this previous knowledge, the quality of cluster separation and the optimal number of clusters can be determined statistically in the following steps:

(i) Calculation of the mean number of maximum possible or actually existing 'overlaps' for all cluster combinations.

(ii) Testing whether the calculated mean values have the same basis (Student's t test). If the null hypothesis, which states that the mean values have the same basic sample, is not rejected, a statistically based separation of the clusters from each other will not be possible. Otherwise, it is possible to proceed as follows:

(iii) For each actual number of 'overlaps' among the clusters, a corresponding ratio number related to the maximum possible number of 'overlaps' is determined: $v_{a,b,} = U_{a,b,} / U_{a,b\ \max}$.

(iv) Calculation of the mean value v over all $v_{a,b;}$

(v) For the reasons stated in (ii), it must be valid for all $v_{a,b} < v$ that its separation as regards the clusters is statistically significant. This is not valid for all $v_{a,b} > \bar{v}$.

(vi) Testing of the frequency of occurrence $U_{a,b}$ against the mean frequency of occurrence U_{m} of 'overlaps' by means of an adjusted χ^2 test with the degree of freedom (DF) = 1:

$$x^2 = \left[(U_{a,b} - U_{\mathrm{m}})^2 \times (2U_{a,b\,\max} - 1)\right] / \left[(U_{a,b} + U_{a,b\,\max}) \times (2U_{a,b\,\max} - U_{a,b} - U_{\mathrm{m}})\right] \tag{A3}$$

The evidence of the test is the following: if the calculated χ^2 values is above a given significance value, the frequency of 'overlaps' above the mean value deviates significantly from it. That means that the separation between the clusters is not statistically safe. Otherwise the separation is statistically safe.

(vii) Now, the initial number of clusters must be varied until at least a single statistically reliable separation between one cluster and the rest exists. If this is fulfilled, the elements of the separated cluster are noted as being a partial final result; and the initial series can be reduced by the separated cluster elements. This algorithm must be repeated until all clusters are separated. An optimal number of clusters is a result of the amount of clusters separated per algorithm step.

APPENDIX B

The fist derivative Gaussian (FDG) and the Haar wavelet transform (Davis *et al.*, 1994; Katul *et al.*, 1994)—the continuous wavelet transform coefficients $W(a,b)$ of a real square integrable single $f(x)$ with respect to a real integrable analysing wavelet $g(x)$ are defined as

$$W(a,b) = (C_g a)^{-1/2} \int_{-\infty}^{\infty} f(t)\, g[(t-b)/a]\mathrm{d}t \tag{B1}$$

where $W(a,b)$ represents the wavelet transform function, or so-called wavelet coefficients, of the raw data function $f(t)$, $a (a > 0)$ is the scale parameter—a larger a value corresponds to a longer time-scale or a lower fluctuation frequency. The $(C_g a)^{-1/2}$ is an energy normalization term, which keeps the energy of the scaled 'daughter wavelet' equal to the energy of the 'mother wavelet' and b is the location parameter; C_g is defined by

$$C_g = \int_{-\infty}^{\infty} H^2(k)\mathrm{d}k/[k] < \infty \tag{B2}$$

where k is the wavenumber and $H(k)$ is the Fourier transform of $g(x)$ given by

$$H(k) = \int_{-\infty}^{\infty} g(x)\, \exp(-ikx)dx. \tag{B3}$$

The condition in equation (B2) ensures the locality of C_g in the Fourier domain. The function $g(x)$ satisfies

$$\int_{-\infty}^{\infty} g(x)\, \mathrm{d}x = 0. \tag{B4}$$

This condition means that the area covered by the wavelet envelope is zero, and ensures that the shape of the wavelet function is always in proportion of the parameters a and b while they vary. The first derivative Gaussian (FDG) function used in this study is

$$g(x) = (\pi/2)^{1/2} \times 4x \times \exp(-2x^2). \tag{B5}$$

The Haar wavelet function used in this study is

$$g(x) = \begin{cases} -1, & \text{for } -1 < x \leq 0, \\ 1, & \text{for } 0 < x \leq 1, \\ 0, & \text{for } |x| > 1 \ldots \end{cases} \tag{B6}$$

where $x = (t - b)/a$ in equations (B5) and (B6). Here the scale parameter a corresponds to a half-cycle of the fluctuation.

REFERENCES

Bernhardt, K. H. and Mäder, C., 1987. 'Statistische Auswertung von Berichten über bemerkenswerte Witterungsereignisse seit dem Jahre 1000', *Z. Meteorol.*, **37**, 120–130.

Berger W. H. and Labeyrie, L. D. 1987. 'Abrupt climactic change an introduction'. Berger W. H. and Labeyrie, L. D. (eds), *Abrupt Climactic Change, Evidence and Implications*, NATO ASI series. *Mathematical and Physical Sciences*, vol 216. D. Reidel, Dordrecht, pp. 3–22.

Brooks, C.E.P. 1927. 'Periodicities in the Nile floods', *Mem. R. Meteorol. Soc.*, **II**, 9–26.

Brunet, Y. and Collineau, S. 1994. 'Wavelet analysis of diurnal and nocturnal turbulence above a maize crop', (eds) in Foufoula-Georgiou, E. and Kumar, P., *Wavelets in Geophysics*, Academic Press, Sand Diego, 129–150 pp.

Collineau, S. and Brunet, Y. 1993. 'Detection of turbulent coherent motions in a forest canopy, Part I: wavelet analysis', *Bound. Layer Meteorol.*, **65**, 357–379.

Conway, D. and Hulme, M. 1993. 'Recent fluctuation in precipitation and runoff over the Nile sub-basins and their impact on main Nile discharge', *Climate Change*, **25**, 127–151.

Currie, R. G. 1987. 'On bistable phasing of 18·6-year induced drought and flood in the Nile records since AD 650', *J. Climatol.*, **7**, 373–389.

Davis, A. Marshak, A. and Wiscombe, W. 1994. 'Wavelet-based multifractal analysis of non-stationary and/or intermittent geophysical signals', in Foufoula-Georgiou, E. and Kumar, P. (eds), *Wavelets in Geophysics*, Academic Press, San Diego, pp. 249–298.

Evans, T. E. 1990. History of the Nile flows, in Howel, P. D. and Allan, J. A. (eds), *The Nile—Resource Evaluation, Resource Management, Hydropolitics and Legal Issues*, Conference at the Royal Geographical Society, University of London, pp. 5–40.

Folland, C. K., Palmer, T. W. and Parker, D. E. 1986. Sahel rainfall and worldwide sea temperatures, 1901–85', *Nature*, **320**, 602–607.

Fraedrich, K. and Bantzer, Ch. 1991. 'A note of fluctuations of the Nile River flood levels (715–1470)', *Theor. Appl. Climatol*, **44**, 167–171.

Gamage, N. K. K. and Hagelberg, C. 1993. 'Detection and analysis of microfronts and associated coherent events using localized transforms', *J. Atmos. Sci.*, **50**, 750–756.

Gerstengarbe, F. -W. and Werner, P. C. 1989. 'A method for the statistical definition of extreme value regions and their application to meteorological time series', *Z. Meteorol.*, **39**, 224–226.

Gerstengarbe, F. -W. and Werner P. C. 1997. 'A method to estimate the statistical confidence of cluster seperation', *Theor. Appl. Climatol.*, **57**, 103–110.

Goossens, C., and Berger, A. 1987. 'How to recognize an abrupt climatic change?' in Berger, W. H. and Labeyrie L. D. (eds), *Abrupt Climatic Change, Evidence and Implications*, NATO ASI series C: *Mathematical and Physical Sciences*, Vol. 216, D. Reidel, Dordrecht pp. 31–46.

Hagelberg, C. R. and Gamage, N. K. 1994. 'Applications of structure preserving wavelet decompositions to intermittent turbulence: a case study', in Foufoula-Georgiou, E. and Kumar, P. (eds),*Wavelets in Geophysics*, Academic Press, San Diego, pp. 45–80.

Hameed, S. 1984. 'Fourier analysis of Nile flood levels', *Geophys. Res. lett.*, **1**, 843–845.

Hassan, F. A. 1981. 'Historical Nile floods and their implications for climate change', *Science*, **212**, 1142–1144.

Hassan, F. A. and Stucki, B. R. 1987. Nile floods and climate change, in Rampino, M. R., *et al.* (eds), *Climate: History, Periodicity, and Predictability*, Van Nostrand, pp. 37–46.

Hurst, H. E., Black, R. P. and Sinaika, Y. M. 1965. *Long Term Storage in Reservoirs. An Experimental Study.*, Constable, London. 145 pp.

Jiang, J. and Liu, R. 1993. 'An analysis of climate jump in the seasonal and annual atmospheric drought indexes over China', *Acta Meteorol. Sin.*, **51**, 237–240. (In Chinese.)

Jiang, J. and Qian, C. 1994. 'An analysis of persistence of 500 hPa pentad mean height anomalies for the Northern Hemisphere Summer', *Chin. J. Atmos. Sci.*, **18**, 185–191.

Jiang, J. and You, X. 1997. 'Where and when did an abrupt climatic change occur in China during the last 43 years?', *Theor. Appl. Climatol.*, in press.

Karl, T. R. and Riebsame, W. E. 1984. 'The identification of 10- to 20-year temperature and precipitation fluctuations in the contiguous United States', *J. Clim. Appl. Meteorol.*, **23**, 950–966.

Katul, G. G., Albertson, J. D., Chu, C. R. and Parlange, M. B. 1994. 'Intermittency in atmospheric surface layer turbulence: the orthonormal wavelet representation', in Foufoula-Georgiou, E. and Kumar, P. (eds), *Wavelets in Geophysics*, Academic Press, San Diego, pp. 81–105.

Kushnir, Y. 1994. 'Interdecadal variations in North Atlantic sea surface temperature and associated atmospheric conditions', *J. Climate*, **7**, 141–157.

Mahrt, L. 1991. 'Eddy asymmetry in the sheared heated boundary layer', *J. Atmos. Sci.*, **48**: 472–492.
Mallat, S. and Zhong, S. 1992. 'Characterization of signals from multiscale edge', *IEEE, Trans. PATTERN Anal. Mach. Intel.*, **14**, 710–732.
Popper, W. 1951. *The Cairo Nilometer*, The University of California Press, Berkley, 269 pp.
Quinn, W. H. 1992. 'A study of Southern Oscillation-related climatic activity for A.D. 622–1900 incorporating Nile River flood data', in Diaz, H. F. and Markgraf, V. (eds), *El Niño: Historical and Paleoclimatic Aspects of the Southern oscillation*, Cambridge University Press, Cambridge, 476 pp.
Riehl, H. and Meitin, J. 1979. 'Discharge of Nile River: a barometer of short-period climate variation', *Science*, **206**, 1178–1179.
Said, R. 1993. *The River Nile, Geology, Hydrology and Utilization*, Pergamon Press, Oxford, 320 pp.
Sneyers, R. 1975. *Sur l'analyse statistique des séries d'observation*, WMO TN 143, World Meteorological Organization Geneva.
Steinhausen, D. and Langer, K. 1977. *Clusteranalyse*, Walter de Gruyter, Berlin, 206 pp.
Stuiver, M. and Quay, P. D. 1980. 'Changes in atmospheric carbon-14 attributed to a variable Sun', *Science* **207**, 11–19.
Toussoun, Prince Omar, 1925. *Mèmoire sur l'histoire du Nil*, MIE, Vol. IX, Cairo.
Whetton, P. D. Adamson, and Williams, M. 1990. 'Rainfall and river flow variability in African, Australia and East Asia linked to El Niño–Southern Oscillation events', *Geol. Soc. Aus. Proc.*, **1**, 71–82.
Yamamoto, R., Iwashima, T. Sanga, N. K. and Hoshiai, M. 1986. 'An analysis of climate jump', *J. Meteorol. Soc. Jpn*, **64**, 273–281.

